UNIVERSITÀ DEGLI STUDI DI MESSINA

Dipartimento di Scienze Biomediche, Odontoiatriche

e delle Immagini Morfologiche e Funzionali

CORSO DI DOTTORATO IN BIOINGEGNERIA APPLICATA ALLE SCIENZE MEDICHE

XXXVI CICLO – MED/36

THE PROGNOSTIC ROLE OF A NEW DEEP LEARNING ALGORITHM FOR THE QUANTIFICATION OF EPICARDIAL ADIPOSE TISSUE VOLUME THROUGH CMR IMAGES IN CORONARY ARTERY DISEASE

Tutor:

Chir.mo Prof. Michele GAETA

Co-Tutor:

Prof. Gianluca PONTONE

Tesi di Dottorato di:

Dott.ssa Maria Ludovica CARERJ

Matricola 522298

Anno Accademico 2022/2023

INDEX

INTRODUCTION

Epicardial adipose tissue (EAT) represents the fat deposit located between the myocardium and the visceral pericardial layer. Human epicardial fat is a metabolically active organ and a source of several bioactive molecules which have numerous exocrine and paracrine effects.[1,2]

Pericoronary adipose tissue (PCAT) of the EAT directly surrounds the coronary arteries. It has a complex bidirectional interaction with the underlying vascular wall.[3] In physiological conditions it is fundamental in maintaining the homeostasis of the vascular wall; while when dysfunctional (e.g., in inflammatory conditions) it plays a key role in the development and progression of atherosclerosis by the production of bioactive molecules (pro-inflammatory cytokines, adipocytokines, growth factors, etc.).[3]

Over the past two decades, EAT has become the subject of increasing scientific investigation, with emerging evidence that it may be associated with the development of coronary artery disease (CAD) and major cardiovascular events.[1,4–6]

Therefore, in an attempt to improve cardiovascular risk assessment, noninvasive imaging has been used increasingly to characterize EAT.

Echocardiography was the first method used for the assessment of EAT, by measuring its thickness along the free wall of the right ventricle.[7]

Cardiac magnetic resonance (CMR) is considered the reference modality for imaging total body fat. CMR provides excellent visualization of the visceral and parietal pericardium enabling easy assessment and volumetric quantification of EAT.

In the recent years applications of artificial intelligence in cardiac imaging have increasingly developed, thus enabling EAT to be quantified faster.[8,9]

In this study we propose a fully automated quantification of EAT based on the analysis of standard routinely acquired CMR cine images. Moreover, we demonstrate that EAT calculated with this tool and indexed for the body mass index (BMI) is a reliable method for predicting myocardial infarction and cardiac death more effectively than other clinical and imaging variables.

Our method does not require the administration of contrast agents. If further validated in other cohorts of patients, it could be applied in the CMR clinical routine to assess the risk of adverse cardiovascular events non-invasively and without the use of contrast agents or ionizing radiation.

1. ANATOMY

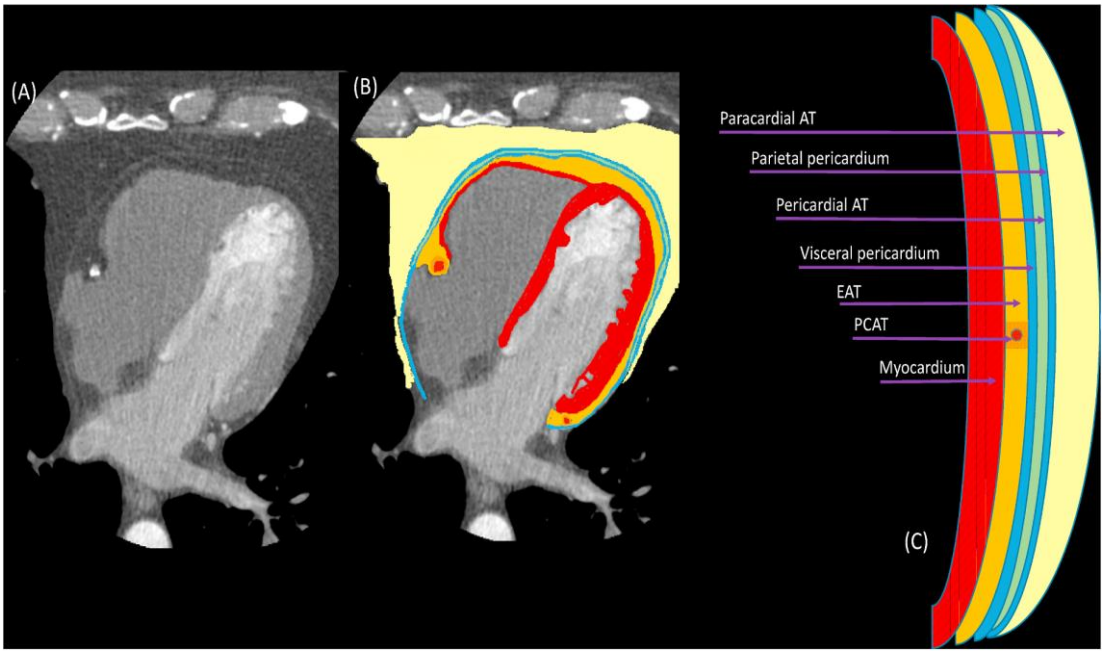

Figure 1. *Anatomy of the adipose tissue surrounding the heart.*

The adipose tissue (AT) surrounding the heart can be divided into (**Figure 1**):

(1)-EAT is the fat deposit located between the myocardium and the visceral layer of the pericardium, supplied by branches of the coronary arteries, which is mostly located in the atrioventricular and interventricular grooves, and can be differentiated into pericoronary EAT (located directly around or on the coronary artery adventitia), and myocardial EAT;

(2)-Pericardial Adipose Tissue (PAT) is located externally and is supplied by non-coronary arteries.

(3)-Paracardial Adipose Tissue is located externally to the parietal pericardium.

EAT is composed mainly of adipocytes but also contains nerve cells, inflammatory cells (mainly macrophages and mast cells), stromal cells, vascular cells and immune cells.

Due to the absence of a muscle fascia between EAT and the myocardium, these two tissues share the same microcirculation. This is unique characteristic of EAT; no other visceral fat deposit has this contiguity with the target organ, without an anatomical barrier, allowing a crosstalk between EAT and the contiguous myocardium.

Interestingly, epicardial and intra-abdominal fat deposits both evolve from brown adipose tissue.[10]

EAT function and morphology change with age and under pathological conditions.

In the childhood EAT is morphologically and functionally similar to brown adipose protecting the heart during unfavourable haemodynamic conditions such as ischaemia or hypoxia.

During adulthood, EAT function changes from thermogenesis to energy storage because the proportion of brown adipocytes decreases in favour of more unilocular white adipocytes, more susceptible to environmental, metabolic and haemodynamic factors, changing the function.

In patients with advanced or end stage organ disease, such as cardiac diseases, and in elderly individuals, the thermogenic function of EAT can be further decreased, with reciprocal increases in the expression of genes encoding profibrotic and proapoptotic factors.

In pathological conditions, such as coronary artery disease, diabetes mellitus, heart failure and atrial fibrillation, EAT becomes proatherogenic and proarrhythmogenic (**Figure 2**).

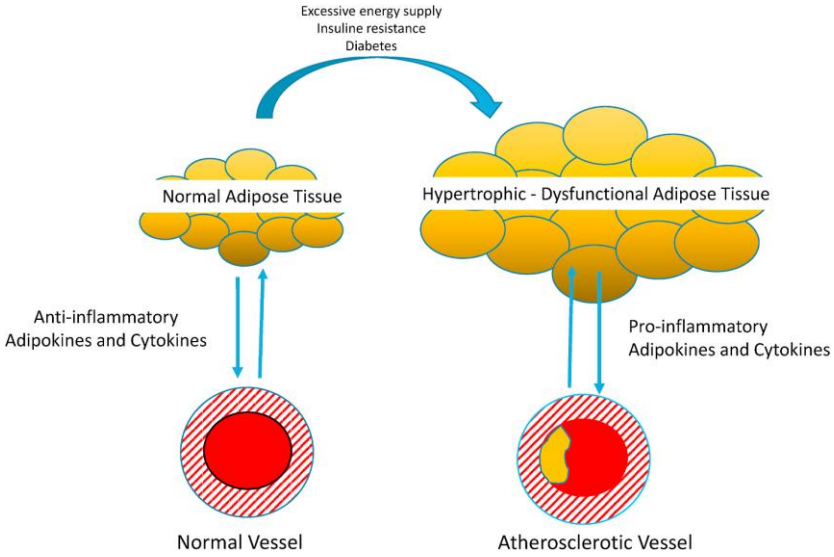

***Figure 2**. EAT/PTCA in normal and pathological conditions.*

2. ROLE OF EAT IN CARDIOVASCULAR DISEASE

2.1. Coronary artery disease

In the early 2000s EAT was first documented to be involved in the multifaced pathways causing coronary atherosclerosis.

The mechanisms through which EAT can cause atherosclerosis are complex and include inflammation, innate immunity iperresponse, oxidative stress, endothelial damage, adipocyte stress, lipid accumulation and glucotoxicity.[11]

In patients with coronary artery disease, coronary epicardial adipose tissue (EAT) has a dense inflammatory infiltrate with a high prevalence of pro-inflammatory M1 macrophages. Coronary EAT secretes proinflammatory cytokines (such as CCL2, IL-6 and tumour necrosis factor (TNF) and adipokines, such as chemerin, intelectin 1, also known as omentin 1, resistin and serglycin), into the coronary lumen, thereby contributing to systemic inflammation.[12–14] Coronary EAT inflammation also contributes locally to coronary atherosclerotic plaque inflammation. The upregulation in the coronary EAT of innate immune response signalling, such as JUN N-terminal kinase (JNK), nuclear factor-κB (NF-κB) and Toll- like receptor (TLR) signalling, can also induce the secretion of inflammatory mediators from the coronary EAT. The excessive production of free fatty acids (FFAs) mediated by group II secretory phospholipase A2 (sPLA2-II), and adipocyte fatty acid binding protein (also known as FABP4) from epicardial adipocytes might infiltrate the adventitia and contribute to the lipid build-up in coronary artery atherosclerotic plaques.[12–14]

The co-occurrence of coronary artery disease with chronic hyperglycaemia can upregulate signalling via advanced glycation end products (AGE) binding to their

receptor RAGE and reduce levels of glucose transporter type 4 (GLUT4), thereby contributing to oxidative stress and endothelial cell damage.[12–14]

EAT assessment can, therefore, help to predict the risk of major coronary events, in this setting the use of imaging techniques for the assessment of EAT could be implemented as routine procedures for effective prediction and stratification of coronary artery disease (CAD).

2.2. Atrial Fibrillation

Atrial fibrillation increases the risk of heart failure, stroke and all-cause death.[15] EAT has emerged as a risk factor and independent predictor of atrial fibrillation development and recurrence after ablation.

The pathogenic role of EAT in atrial fibrillation could begin with its embryogenesis. Embryonic epicardium can generate coronary smooth muscle cells and cardiac fibroblast or undergo adipogenic differentiation.[16] Atrial EAT adipocytes originate from the differentiation of progenitor cells resident in the epicardium and from the secretome of atrial myocytes.[14,16]

Peri-atrial EAT has a specific gene expression signature compared with periventricular and pericoronary EAT.[14,17]

EAT infiltrating the atrium has increased expression of genes encoding proteins involved in oxidative phosphorylation, muscular contraction and calcium signalling compared with periventricular and pericoronary.[14,17]

The absence of a fascia separating peri-atrial EAT from the underlying left atrial myocardium and a shared blood supply provide a milieu for bidirectional communication.

Pro-inflammatory and profibrotic cytokines, such as interleukins and TNF, and profibrotic factors, such as matrix metalloproteinases (MMPs) and activin A, can diffuse from EAT into the adjacent atrial myocardium and promote arrhythmias.[14,17]

Fibrosis also has an important pathogenic role in the development of atrial fibrillation.[18]

EAT can also influence the local electrophysiological properties of the atrial and pulmonary veins, such as the refractory period, and therefore sustain atrial fibrillation.[19]

Investigations with cultured human induced pluripotent stem cell-derived cardiomyocytes indicate that local peri-atrial EAT accumulation, rather than global cardiac adiposity, contributes to conduction abnormalities underlying the atrial fibrillation substrate.[14,20]

Peri-atrial EAT accumulation can slow conduction and prolong cardiomyocyte field potential duration through two mechanisms: by physical conduction block caused by extensive fibrosis, and by local EAT infiltration of the adjacent atrial myocardium, which causes conduction heterogeneity and electrophysiological changes through the paracrine release of cytokines that induce inter-cardiomyocyte adhesion disruption and abnormal cell coupling, alter ionic currents and myocardial metabolism, and promote inflammation.[20,14]

EAT contains sympathetic and parasympathetic nerve fibers that contribute to overall cardiac autonomic neuronal output.

Interestingly, botulinum injection into EAT during cardiac surgery can suppress ganglionated plexi, reduce autonomic[21] nervous activity and have long-term beneficial effects on atrial fibrillation.[14]

The infiltration of adipocytes into the atrial myocardium disorganizes the depolarization wavefront, inducing micro re-entry circuits and local conduction blocks.[14]

EAT thickness and volume are greater in patients with persistent atrial fibrillation, than in those with paroxysmal atrial fibrillation independent of obesity, age, sex, or presence of CAD, diabetes, dyslipidaemia or hypertension.[14,22,23] Several studies have highlighted the use of EAT measurement in predicting outcomes after catheter ablation for paroxysmal or persistent atrial fibrillation.[21,24,25] Peri-atrial EAT volume is greater in patients with atrial fibrillation and is associated with recurrence after catheter ablation.[14,24,25] EAT volume is associated with atrial fibrillation persistence independent of other risk factors or BMI.[26]

2.3. Heart failure

EAT has been suggested to have a role in heart failure, particularly in patients with preserved ejection fraction (HFpEF).[14,27–29] The volume of EAT is significantly higher in patients with HFpEF than in healthy individuals.[28,29]

EAT can affect cardiac function in the setting of heart failure via several mechanisms, such as increased inflammation, fibrosis and autonomic dysregulation as well as through the mechanical effects of a large, fibrotic fat pad.[14]

3. ROLE OF IMAGING IN EAT ASSESMENT

Multiple types of equipment can be used to evaluate EAT, including CT, CMR, and echocardiography.[8]

The thickness of EAT can be visualized and measured with standard 2D echocardiography. EAT thickness is measured perpendicularly on the free wall of the right ventricle at end-systole when both walls collapse and allow the widest measurement. EAT is identified as the echo-free space between the outer wall of the myocardium and the visceral layer of the pericardium, but EAT can also appears as an echo-dense space when inflammation or large amounts of EAT are present. [1,14]

Echocardiographic measurement of EAT thickness is a marker of visceral adiposity, and EAT thickness variability (ranging from 1 mm to 25 mm) reflects the variation in intra-abdominal fat accumulation. Even if excellent interobserver and intraobserver agreement is reported, echocardiography is still an operator-dependent technique.[1,8]

Cardiac multidetector CT and cardiac MRI can provide volumetric measurement of EAT and additional functional information by detecting deep regional EAT that is not accessible with transthoracic echocardiography.[9,30]

Visualizing peri-atrial and pericoronary EAT is important in understanding, predicting and possibly preventing the effects of EAT in atrial fibrillation and CAD.[14,24,31]

Both contrast-enhanced and non-contrast-enhanced, cardiac-gated multidetector CT are used to quantify EAT.[14,30]

The combination of high spatial resolution, volume coverage of the entire heart and increasing availability of software analysis tools makes the use of CT to measure EAT ideal. However, differences exist in the CT attenuation (a measure of EAT density, expressed in Hounsfield units (HU)) characteristics of EAT depending on the presence or absence of iodinated contrast and inflammatory status.[14,32] EAT density is a marker of both EAT and general inflammation.[33,34] EAT attenuation ranges between – 45 HU and –195 HU, where a lower negative means higher density.[32–34]

Although 18F-FDG-PET-CT can detect EAT inflammatory activity, this modality is not cost-effective or readily available.[12]

With the increasing potential of AI in disease assessment, the role of AI in the assessment of EAT and PCAT has attracted increasingly more attention.[35]

4. ARTIFICIAL INTELLIGENCE: THEORETICAL MACHINE LEARNING BACKGROUND

4.1. Machine Learning

Machine Learning (ML) is a subfield of artificial intelligence (AI) which is founded on the basis that machines should be able to learn and adapt through experience.[36] Thus, ML is a method of data analysis that automatizes analytical model building.

More precisely, the underlying algorithm is selected or designed by humans, but the algorithm automatically learns from data about the parameters that will shape a mathematical model. In this way, humans do not know how the model is internally built by the machine. [37]Model building starts with the selection of the ML algorithm to use, such as decision trees, support vector machines or artificial neural networks. The algorithm must be chosen based on interpretability, simplicity, accuracy, speed of training, testing, processing and scalability. The starting point for ML process is raw data and the end point is a model derived from that data. The larger is the amount of data, the better the results are likely to be. Moreover, the quality, preparation, and selection of data are critical to the success of an ML solution. According to Mitchell (1997)[38], machines learn by detecting patterns in data and apply known rules to categorise, make predictions, detect anomalous behaviours and identify unknown relationships. More generally, there are two ways in which machines learn: supervised learning, in which models are trained based on input data with the corresponding desired output, and unsupervised learning, where no output labels are provided. Supervised learning problems include classification and regression, while

unsupervised learning is mostly used to automatically discover groups in data (clustering) or extract hidden associations between variables association rules.[39] In the last few years, ML has become much more popular for faster processing of massive amounts of structured, unstructured and semi-structured data. In particular, ML algorithms have been successfully deployed in a large variety of applications such as text analysis, translation, speech recognition, image and video 18 analysis, with an important contribution in the biomedical field and medical diagnosis.

4.2. Deep Learning

Deep Learning (DL) is a subset of ML. DL consists of multiple hidden layers of information existing in an artificial neural network.[40] Essentially, DL attempts to simulate how the human brain processes information. DL can be implemented by means of several different algorithms, all of which are marked by a cascade of many processing layers organized in a hierarchical structure. Each of these layers add a level of abstraction to the overall representation. More precisely, DL obtains a set of features learned directly from observations of the input dataset. Layers close to the input deal with low-level features such as edges and texture in images, while deep layers extract complex higher-level features.[41] Therefore, it is possible to consider the deep layers of a CNN as a feature extractor. The key advantage of DL is that the features are automatically extracted from the data by the neural network, while in ML hand-crafted features are used, designed by experts to extract a given set of chosen characteristics.[42] For DL models, huge amounts of training data is necessary. The advent of the big data era resulted in an increasing use of these methods. Two other key premises were the availability of low-cost machines with powerful arithmetic units and the possibility of

applying the already known learning techniques to nonlinear systems composed of several layers of processing. Another key advantage of DL is represented by transfer learning. The basic concept is that first-layer features appear not to be specific to a particular dataset or task, but general in that they are applicable to many datasets and tasks. On the other hand, features computed by the last layer of a trained network depend greatly on the chosen dataset and task. Thus, it is possible to first train a base network on a base dataset and task; successively, the learned features can be repurposed or transferred to a second target network to be trained on a different target dataset and task. The remaining layers of the target network are then randomly initialized and trained toward the target task. Then, the errors from the target network can be backpropagated into the base (transferred) features to fine-tune them to the new task, or the transferred layers can be left frozen, with no change during training.[43] Some examples in which DL is being employed are automatic language translation, image recognition, spam filtering, fraud detection, computer vision and medical diagnoses.[36]

5. THE PROGNOSTIC ROLE OF A NEW DEEP LEARNING ALGORITHM FOR THE QUANTIFICATION OF EPICARDIAL ADIPOSE TISSUE VOLUME THROUGH CMR IMAGES IN CORONARY ARTERY DISEASE

5.1. Aim of the study

Our study aims:

a) to develop and apply a new deep-learning (DL) algorithm, for fully automated EAT segmentation;

b) to evaluate the prognostic role of EAT volume in CMR images.

5.2. Methods

5.2.1. Study population

This was a retrospective study in a cohort of consecutive patients with suspected or known coronary artery disease (CAD) who were referred for cardiac magnetic resonance (CMR) at "IRCCS Centro Cardiologico Monzino" in Milan.

Between January 2011 and December 2014, 836 patients were evaluated for the study. Exclusion criteria were:

- heart failure or known infiltrative or hypertrophic cardiomyopathy (n=48);
- severe claustrophobia (n=32);
- presence of an implantable device (n=20);

- estimated glomerular filtration rate ≤30 mL/min (n=12), and impaired image quality of CMR images (n=22).

The Institution's ethical committee approved the protocol, and all patients gave their written informed consent.

The clinical variables collected for each patient included demographic data, prior cardiac history (history of CAD or previous revascularization with percutaneous coronary intervention or coronary artery bypass graft), hypertension (blood pressure >140/90 mmHg or use of antihypertensive agents), current or previous smoking, hyperlipidemia (low-density lipoprotein cholesterol LDL >116 mg/dL), diabetes mellitus (fasting glucose level >110 mg/dL or need for insulin or oral hypoglycemic drugs).

All patients were followed from the time of CMR imaging. Outcome events were obtained by clinical visits or telephone interviews; contact with the patient's primary care physician or cardiologist was performed in case of death.

Major adverse cardiovascular events (MACE) were defined as a combined endpoint of:

1) Non-fatal myocardial infarction defined according to the 4th universal definition of myocardial infarction (12) as a rise and/or fall of troponin values with at least 1 value above the 99th percentile upper reference limit (URL) and with at least 1 of the following:

    - Symptoms of acute myocardial ischemia;
    - New ischemic electrocardiographic (ECG) changes;
    - Development of pathological Q waves;

- Imaging evidence of new loss of viable myocardium or new regional wall motion abnormality in a pattern consistent with an ischemic etiology;
- Identification of a coronary thrombus by angiography including intracoronary imaging.

2) Sudden cardiac death defined as symptoms suggestive of myocardial ischemia accompanied by presumed new ischemic ECG changes or ventricular fibrillation, with death before blood samples for biomarkers can be obtained, or before increases in cardiac biomarkers can be identified, or myocardial infarction is detected by autopsy examination.[9]

5.3. CMR Protocol

CMR studies were performed with a 1.5-T Discovery MR450 (G.E. Healthcare, Milwaukee, Wisconsin). Studies used dedicated cardiac software, phased-array surface receiver coils, and electrocardiogram triggering. Breath-hold steady-state free-precession (SSFP) cine imaging was performed in vertical and horizontal long- and short-axis orientations.

SSFP cine sequences were acquired using the following parameters: echo time 1.57 ms, 15 segments, repetition time 46 ms without view sharing, slice thickness 8 mm, field of view 350×263 mm, and pixel size 1.4×2.2 mm.

A contrast-enhanced breath-hold segmented T1-weighted inversion-recovery gradient-echo sequence was used for the detection of late gadolinium enhancement (LGE).

LGE imaging was performed 10 to 20 min after administration of an intravenous bolus of gadolinium at a flow rate of 4 mL/s followed by saline flush. The inversion time was individually adjusted to null normal myocardium (usual range 220 to 300 ms). The following parameters were used: FOV: 380 to 420 mm; TR/TE: 4.6/1.3 ms; α: 20°; matrix: 256 × 192; slice thickness: 8 mm and no interslice gap.

5.4. CMR Imaging Analysis

CMR datasets were transferred to a dedicated workstation and analyzed with a commercially available cardiac software (Circle CVI42® 5.13.9 software).

The following parameters were measured: left end-diastolic (LVEDV) and end-systolic (LVESV) volumes, left (LVEF) and right (RVEF) ejection fraction; left ventricle mass (LV mass). LVEDV, LVESV, LV mass, RVEDV and RVESV were indexed for the body surface area.

The EAT contours were manually contoured at end-diastole, starting at the mitral valve level and moving upwards to the inferior margin of adipose tissue as previously described[9].

LGE was defined as a myocardial segment with a signal intensity increase >5 S.D., above the mean signal intensity of remote myocardium. The absolute number and percentage of patients with LGE and as well as of myocardial mass showing LGE, were assessed.

All the analyses were performed by four readers with two to four years of experience in CMR and reviewed by two expert readers, with more than 8 years' experience, blinded to the outcome data.

EAT volume index (ml m^2/kg) was defined as the ratio between EAT volume and the patient BMI.

5.5. Deep Learning Analysis

For automated CMR image analysis, a fully-convolutional network architecture[44] was implemented to perform pixelwise segmentation from an input image. The structure of the network was implemented from the UNet[45], which has achieved remarkable success on medical images, and it consists of an encoder-decoder structure to combine high-level semantics with low-level fine-grained surface information.

As shown in **Figure 3**, the network architecture includes two-dimensional (2D) and three-dimensional (3D) branches processing information.

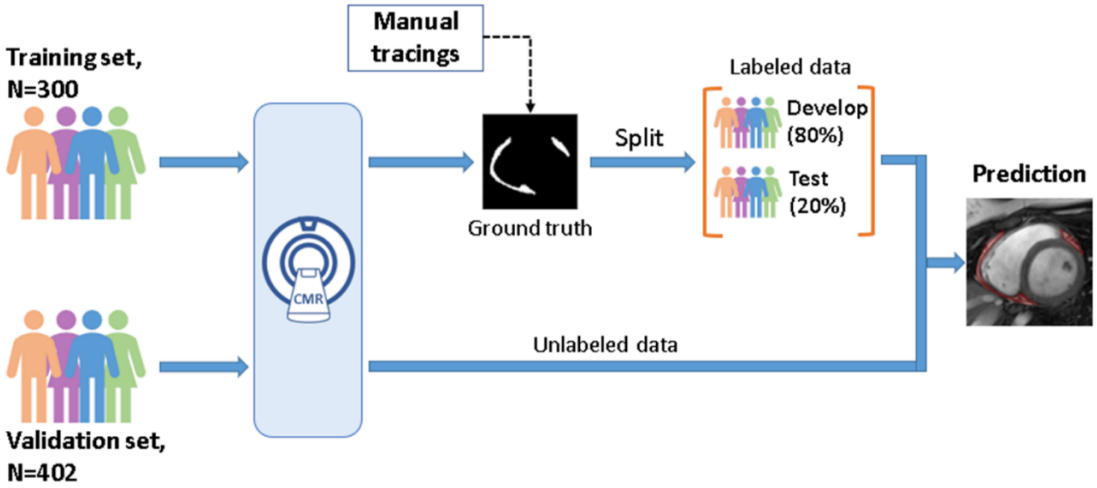

***Figure 3**. Overview of the proposed workflow for automated EAT volume segmentation on short-axis cine CMR images.*

The proposed workflow for EAT volume quantification from short-axis cine images is shown in **Figure 4**.

First, the training set of 300 patients with labeled CMR imaging (ground truth) was randomly split (patient-wise) into development (n=240, 80%) and held-out testing (n=60, 20%) cohorts.

After the model was trained and evaluated, we applied our segmentation network to a validation set of 402 patients with unlabeled data for automated EAT segmentations. Finally, we applied the DL algorithm to the overall study cohort of 702 patients. The obtained measures were then used to assess the prognostic role of EAT over standard clinical and imaging parameters.

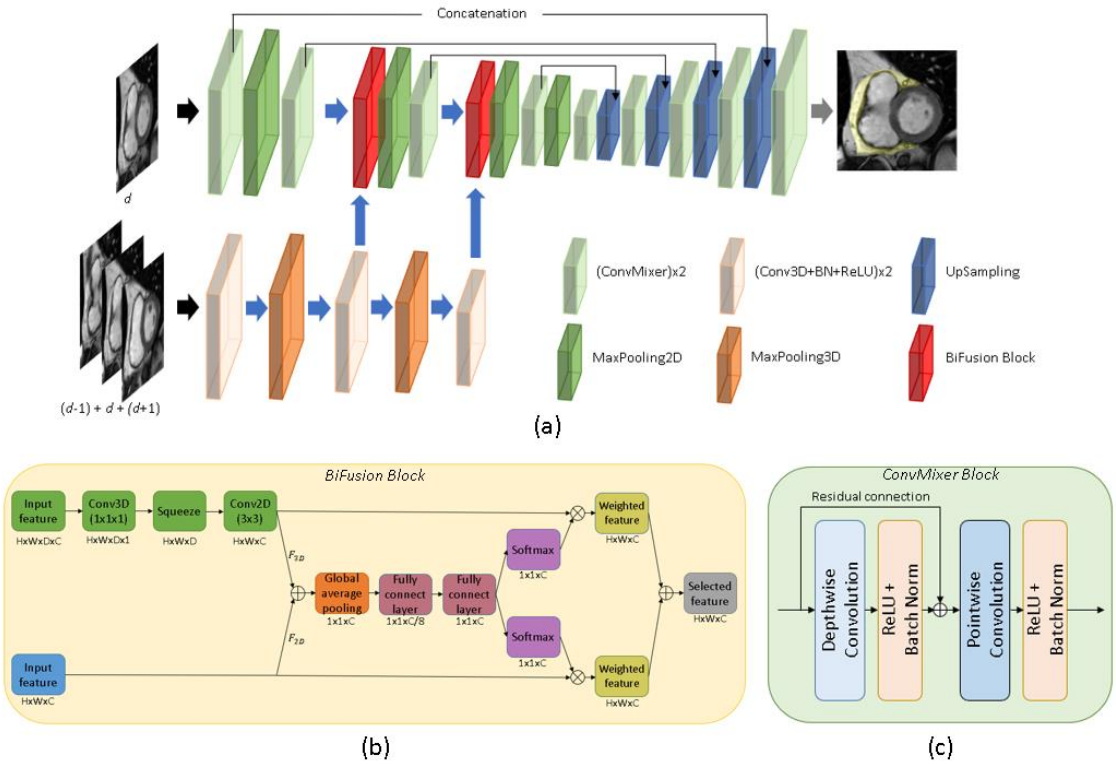

Figure 4*. The main architecture diagram which combines 2D and 3D convolutions for epicardial adipose tissue segmentation from a cardiovascular magnetic resonance cine image.* ***(b)*** *The BiFusion Block which has two branches for its 2D and 3D input* ***(c)*** *ConvMixer Block which is used to extract features from an input image.*

5.6. Statistical Analysis

Continuous variables were reported as mean±SD or median (25^{th}–75^{th} percentile), as appropriate and categorical variables, and as absolute numbers and frequencies. Accordingly, Student's independent t-test, Chi-square, or Fisher's exact, were used to compare the distribution of variables between groups.

Interobserver variability for the evaluation of EAT volume, as well as the performance of human vs. DL, were compared on the test set by using intraclass correlation coefficient (ICC), Bland–Altman analysis and coefficient of variation (CV). The time

to the first event was considered in our analysis. Univariable Cox proportional hazard models were used to assess the association between clinical and imaging data with the risk of MACE (presented as hazard ratio [HR] and 95% confidence interval [CI]).

After correlation examination, variables with $p<0.05$ at univariable analysis were then included as covariates in multivariable Cox proportional hazard models, using a stepwise adjusted approach to test association with MACE events. In addition, the discriminative ability of variables to diagnose MACE was evaluated by Harrell's C statistic and compared with the De-Long test. The cumulative survival rate was assessed with the Kaplan-Meier method for all subjects and compared by log-rank test. EAT volume, as mentioned before, was corrected for body mass index (EAT volume index) and dichotomized into high versus low volume, using a threshold of ≥2.2 mLm^2/Kg determined by maximum Youden's index (defined as sensitivity + specificity -1).

Finally, the incremental prognostic value of CMR variables in predicting MACE by stepwise inclusion of each candidate variable was assessed by the change in likelihood ratio Chi-square using the Omnibus test of model coefficients.

All tests were 2-tailed, and $p<0.05$ was considered statistically significant. Statistical analyses were performed on SPSS (version 27.0) and Python with scikit-learning package (version 0.22.2, https://scikit-learn.org/stable/).

5.7. Results

Seven hundred-two patients (age 63±10 years) were enrolled. The mean follow-up time to event, for patients experiencing events, was 32 months (range, 2–81), while

the mean follow-up duration in patients with no events was 71 months (range, 1–91). No patients were lost to follow-up.

Time to event was calculated as the period between the CMR study and the first occurrence of a MACE.

Fifty-two patients (7.4%) developed MACE during follow-up (41 non-fatal myocardial infarctions and 11 cardiac deaths).

Baseline characteristics of patients with and without MACE are reported in **Table 1**. Prevalence of hypertension, diabetes mellitus, hyperlipidemia, and previous revascularization were higher in patients with events than in those with no events. Patients experiencing MACE were more often treated with beta-blockers, angiotensin-converting enzyme inhibitors, diuretic agents, and statins because they were more complex. No differences were found in terms of demographic characteristics between groups.

As compared to patients without MACE, patients experiencing MACE showed higher LVEDV index (94 ± 34 vs. 82 ± 23 ml/m^2, p =0.016) and LVESV index (51±34 vs. 38±20 ml/m^2 p=0.008), lower LVEF (49.4 ± 15.2 vs. 55.6 ± 11.6 %, p=0.006), and higher per-patient prevalence of LGE (77% vs. 48%, p < 0.001). EAT volume index was significantly higher in patients with MACE than those without (2.3±0.5 vs. 1.9±0.5 mL*m^2/Kg; p=0.003).

Table 1: Baseline Characteristics

	Total Subjects N=702	**MACE** N=52	**NO MACE** N=650	***p*-value**
Demographics				
Age, years	63 ± 10	62 ± 10	63 ± 10	0.417
Male	593(84%)	44(85%)	549(84%)	0.976
BMI, Kg/m^2	26.4 ± 3.6	25.8 ± 3.7	26.1 ± 3.6	0.331
BSA, m^2	1.9 ± 0.2	1.9 ± 0.2	1.9 ± 0.2	0.382
Cardiovascular risk factors				
Family history	129(18%)	8(15%)	121(19%)	0.563
Smoking	188(27%)	19(36%)	169(26%)	0.099
Hypertension	309(44%)	35(67%)	274(42%)	<0.001*
Diabetes mellitus	103(15%)	13(25%)	90(14%)	0.029*
Hyperlipemia	310(44%)	34(65%)	276(42%)	0.001*
CABG	101(14%)	11(21%)	90(14%)	0.149
Previous PCI	466(66%)	47(90%)	419(64%)	<0.001*
Medications				
Beta-blockade	297(42%)	32(61%)	265(41%)	0.004*
ACE inhibitors/AT1 blockers	273(39%)	28(54%)	245(38%)	0.021*
Diuretics	78(11%)	11(21%)	67(10%)	0.017*
Ca-antagonists	100(14%)	8(15%)	92(14%)	0.807
Anti-thrombotic agents	390(56%)	33(63%)	357(55%)	0.233
Nitrates	59(8%)	6(11%)	53(8%)	0.397
Statin	325(46%)	32(61%)	293(45%)	0.022*
Anti-arrhythmic	38(5%)	2(4%)	36(5%)	1.000
CMR characteristics				
LVEDV index (mL/m^2)	83 ± 24	94 ± 34	82 ± 23	0.016*
LVESV index (mL/m^2)	39 ± 21	51 ± 34	38 ± 20	0.008*
LVEF (%)	55.2 ± 12.0	49.4 ± 15.2	55.6 ± 11.6	0.006*
LV mass index (g/m^2)	65 ± 18	71 ± 21	65 ± 18	0.061
RVEDV index (mL/m^2)	68 ± 16	65 ± 16	69 ± 16	0.165
RVESV index (mL/m^2)	27 ± 10	26 ± 11	27 ± 10	0.470
RVEF (%)	62.2 ± 23.7	60.9 ± 8.3	62.3 ± 24.6	0.682
LGE, presence	353(50%)	40(77%)	313(48%)	<0.001*
LGE mass (g)	9.1 ± 14.8	15.0 ± 18.5	8.6 ± 14.3	0.018*
EAT volume (mL)	49.7 ± 18.0	54.0 ± 16.2	68.6 ± 33.6	0.125
EAT volume index≥1.8 mL*m^2/Kg	305(43%)	30(58%)	275(42%)	<0.001*

Results are shown as mean±SD or n(%)

A cohort of 300 patients were used as a training dataset to develop a DL algorithm. The training cohort's baseline characteristics are described in **Table 2**.

Table 2. Baseline Characteristics of the Training Cohort

	Total Subjects N=300	**MACE** N=21	**No MACE** N=279	*p* value
Demographics				
Age, years	63 ± 10	60 ± 10	64 ± 10	0.175
Male	259(86%)	19(90%)	240(86%)	0.563
BMI, Kg/m^2	26.6 ± 3.7	26.0 ± 4.0	26.7 ± 3.7	0.453
BSA, m^2	1.9 ± 0.2	1.9 ± 0.1	1.9 ± 0.2	0.381
Cardiovascular risk factors				
Familiar history	69(23%)	4(19%)	65(23%)	0.649
Smoking	99(33%)	9(43%)	90(32%)	0.325
Hypertension	163(54%)	15(71%)	148(91%)	0.106
Diabetes mellitus	56(19%)	9(43%)	47(17%)	0.003*
Hyperlipidemia	178(59%)	15(71%)	163(58%)	0.249
CABG	42(14%)	5(24%)	37(13%)	0.182
Previous PCI	206(69%)	20(95%)	186(67%)	0.007*
Medications				
Beta-blockers	171(57%)	18(86%)	153(55%)	0.006*
ACE inhibitor/AT1 blockers	159(53%)	13(62%)	146(52%)	0.406
Diuretics	51(17%)	5(24%)	46(16%)	0.394
Ca-antagonists	54(18%)	3(14%)	51(18%)	0.641
Anti-thrombotic agents	225(75%)	18(86%)	207(74%)	0.249
Nitrates	47(16%)	5(24%)	42(15%)	0.291
Statin	189(63%)	19(90%)	170(61%)	0.007*
Anti-arrhythmic	22(7%)	1(5%)	21(7%)	1.000
CMR characteristics				
LVEDV index (mL/m^2)	82 ± 23	87 ± 22	81 ± 23	0.304
LVESV index (mL/m^2)	37 ± 21	44 ± 24	37 ± 20	0.093
LVEF (%)	56.5 ± 12.0	51.3 ± 14.9	56.9 ± 11.7	0.041*
LV mass index (g/m^2)	60 ± 12	64 ± 13	60 ± 12	0.136
RVEDV index (mL/m^2)	68 ± 15	61 ± 12	68 ± 15	0.030*
RVESV index (mL/m^2)	26 ± 9	23 ± 6	26 ± 9	0.112
RVEF (%)	64.1 ± 35.7	61.9 ± 9.0	64.3 ± 37.0	0.763
LGE, presence	150(50%)	16(76%)	134(48%)	0.013*
LGE mass (g)	7.0 ± 12.2	7.9 ± 9.6	6.9 ± 12.3	0.732
EAT volume (mL)	57.0 ± 17.2	61.4 ± 13.1	56.7 ± 17.4	0.224
EAT volume index mL*m^2/Kg	2.1 ± 0.6	2.4 ± 0.6	2.1 ± 0.6	0.051*
EAT volume index≥2.2 mL*m^2/Kg	214(71%)	20(95%)	194(69%)	0.010*

Figure 3 shows the Bland–Altman plots of the EAT volume and compares automated segmentation to manual segmentation and segmentations by different human observers on the test set. The automated method was shown in a strong correlation (ICC = 0.90) with limited bias and narrow limits of agreement, demonstrating that for the EAT volume, the computer-human difference is comparable with the human-human difference.

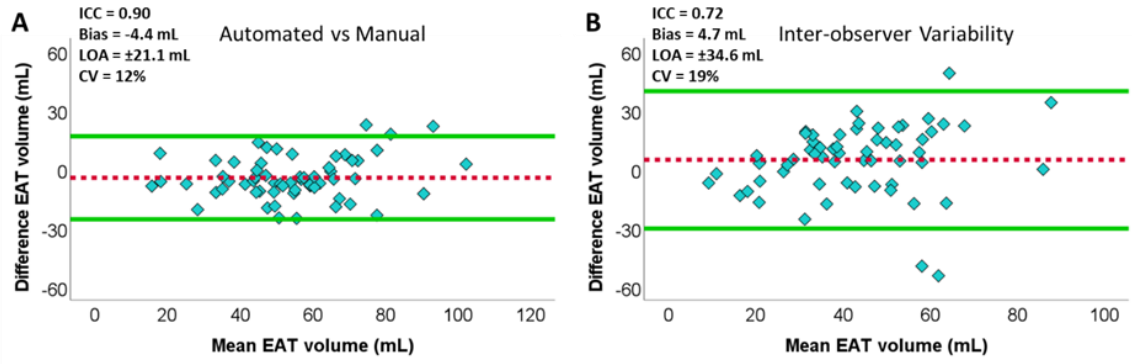

Figure 3*. Bland Altman plots.*

Mean analysis time of a single subject for the automated method was significantly faster than the manual approach (0.4 sec vs. 249 sec, p=<0.001).

Examples of EAT segmentation results of our proposed network on short-axis cine CMR images are illustrated in **Figure 5**.

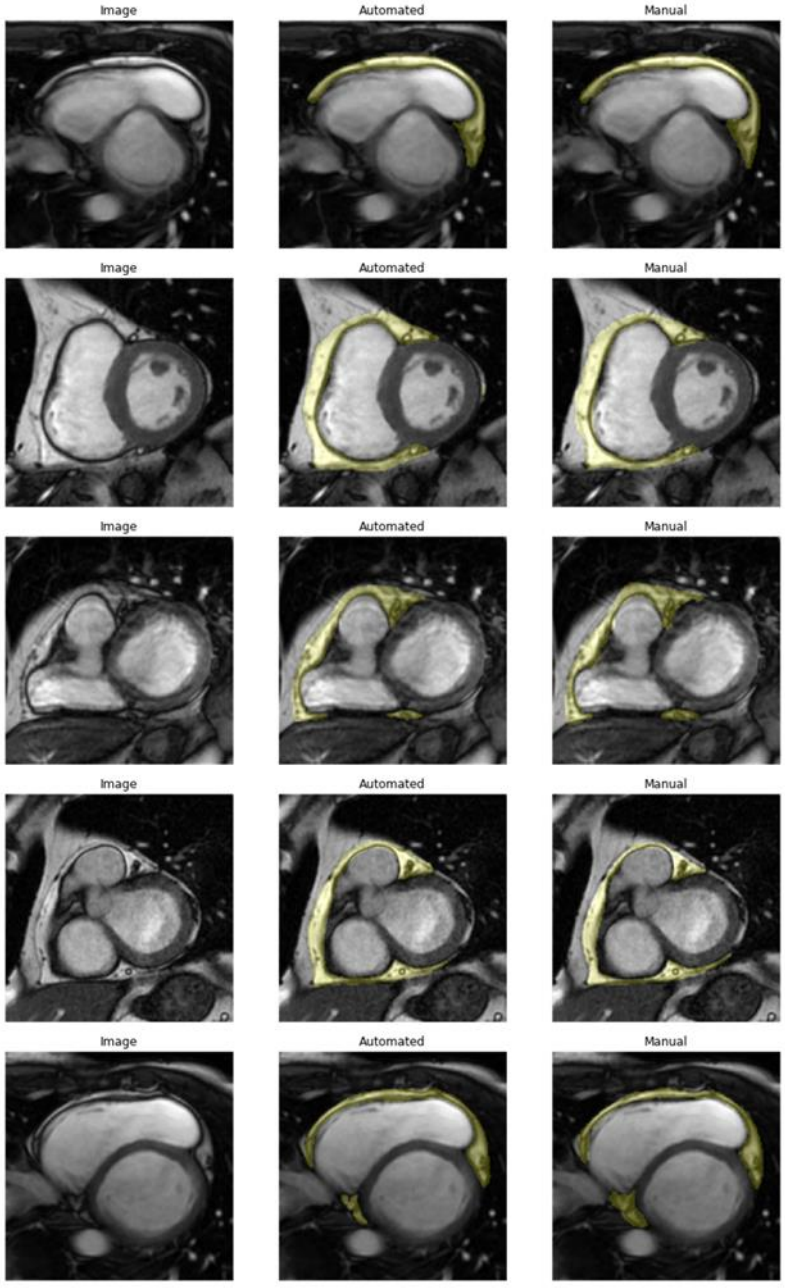

Figure 5. *Example of segmentation results of the epicardial adipose tissue on cardiac magnetic resonance short-axis cine images using the proposed network compared to the manually traced contours.*

Table 3. Univariable and Multivariable Cox model for MACE

	Univariable analysis		Multivariable analysis	
	HR (95% CI)	***p* value**	**HR (95% CI)**	***p* value**
Demographics				
Age	0.991 (0.966-1.016)	0.457		
Male	1.018 (0.479-2.162)	0.963		
BMI	0.951 (0.863-1.048)	0.309		
BSA	0.449 (0.078-2.579)	0.369		
Cardiovascular risk factors				
Familiar history	0.758 (0.356-1.611)	0.471		
Smoking	1.567 (0.891-2.757)	0.119		
Hypertension	2.646 (1.480-4.728)	0.001		
Diabetes mellitus	2.016 (1.076-3.778)	0.029		
Hyperlipidemia	2.333 (1.315-4.140)	0.004		
CABG	1.728 (0.888-3.363)	0.107		
Previous PCI	5.086 (2.023-12.788)	0.001		
Medications				
Beta-blockade	2.092 (1.194-3.665)	0.010		
ACE inhibitor/AT1 blockers	1.761 (1.019-3.045)	0.043		
Diuretics	2.111 (1.083-4.113)	0.028		
Ca antagonists	1.102 (0.519-2.342)	0.800		
Anti-thrombotic agents	1.300 (0.737-2.295)	0.365		
Nitrates	1.323 (0.564-3.105)	0.520		
Statin	1.780 (1.016-3.119)	0.044		
Anti-arrhythmic	0.682 (0.166-2.804)	0.596		
CMR characteristics				
LVEDV index	1.017 (1.008-1.026)	<0.001		
LVESV index	1.020 (1.012-1.029)	<0.001		
LVEF ≤50%	2.046 (1.184-3.538)	0.010	1.939 (1.093-3.441)	0.024
LV mass index	1.017 (1.002-1.032)	0.028		
RVEDV index	0.987 (0.969-1.005)	0.167		
RVESV index	0.990 (0.961-1.020)	0.516		
RVEF	0.989 (0.954-1.026)	0.553		
LGE, presence	3.426 (1.797-6.532)	<0.001	2.806 (1.439-5.473)	0.002
LGE mass (g)	1.022 (1.009-1.036)	0.001		
EAT volume (mL)	1.011 (0.997-1.026)	0.135		
EAT volume index	3.032 (1.910-4.815)	0.018		
EAT volume index ≥2.2	5.324 (1.623-17.462)	0.006	7.890 (4.385-14.195)	<0.001

The **Table 3** shows the hazard ratio (HR) of various risk factors on MACE by univariate and stepwise multivariable Cox proportional hazards model analysis of the overall population. MACE was significantly associated with EAT volume index. The HR was higher in patients with reduced LVEF (≤50%), left ventricle dilation, LGE, hypertension, diabetes, hyperlipemia, and with previous percutaneous

revascularization. Regarding medical therapy, beta-blockers, angiotensin-converting enzyme inhibitors, diuretic agents, and statins were also predictors of MACE, because they were mainly administered in more complex patients.

In multivariable analysis, EAT volume index was the strongest independent predictor of MACE (HR: 7.890; 95% CI: 4.385-14.195), along with LVEF (HR: 1.939; 95% CI: 1.093-3.441) and LGE detection (HR: 2.806; 95% CI: 1.439-5.473).

Finally, the incremental value in predicting the endpoint by stepwise inclusion of LGE and EAT volume index, in addition to LVEF, is shown in **Figure 6**.

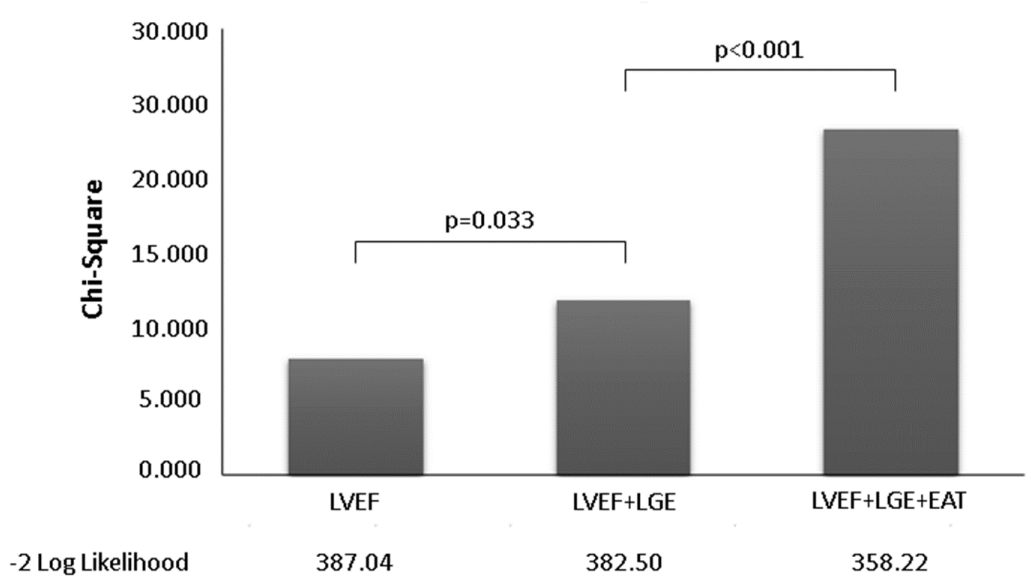

***Figure 6**. Chi-Square Improvement Analysis. Incremental value in predicting outcome by stepwise inclusion of late gadolinium enhancement (LGE) and epicardial adipose tissue (EAT) volume index in addition to left ventricular ejection fraction (LVEF).*

The addition of LGE to LVEF was identified as an incremental predictor of events (p=0.033), with further enhancement when EAT volume index was added to the model (p<0.001). Adding EAT volume index in the presence of LGE to the model, including LVEF, provided an improvement in predicting the endpoint with a Harrell C statistic of 0.75 (**Figure 7**).

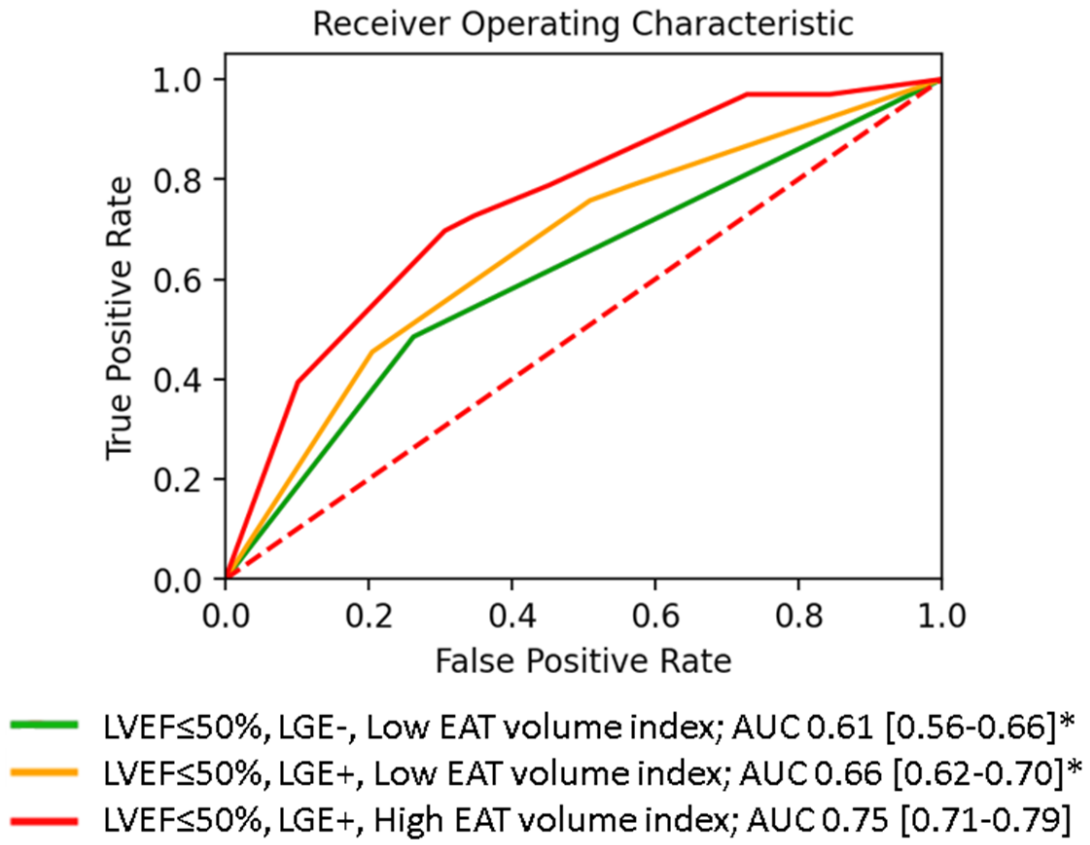

Figure 7*. The figure shows a more AUC with the model LVEF<= 50%, LGE+, High EAT volume index.*

In the **Figure 8** are reported the Kaplan-Meier survival curves for MACE, according to LVEF (Panel A), LGE detection (Panel B), EAT volume index (Panel C), and their combination (Panel D). Event-free survival rate was 77% for high-risk patients (i.e., with reduced LVEF, LGE, and high EAT volume index); 92% for intermediate-risk patients (i.e., reduced LVEF, LGE, low EAT volume index); and 96% for low-risk patients (i.e., reduced LVEF, without LGE, low EAT volume index).

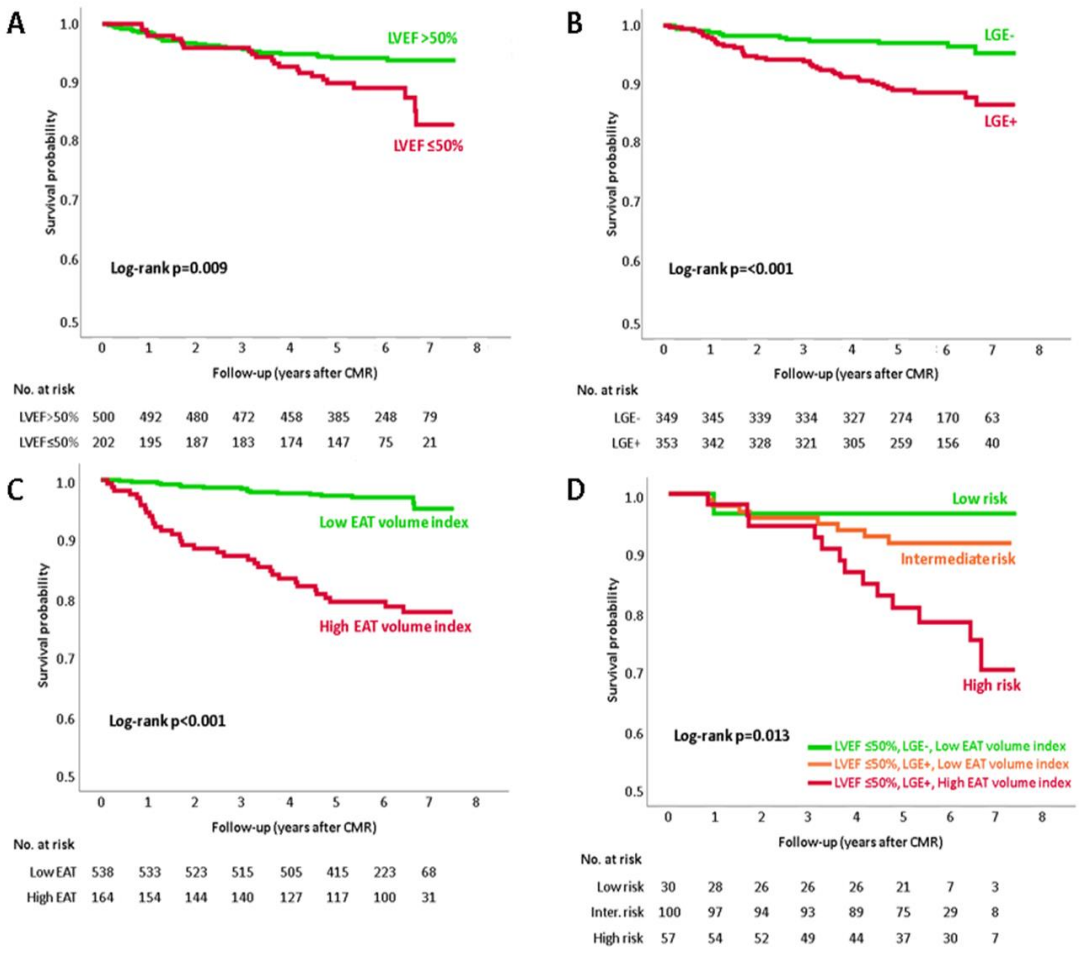

***Figure 8**. Kaplan–Meier curves for major adverse cardiac events (MACE) based on left ventricle ejection fraction (LVEF; **A**), late gadolinium enhancement (LGE) detection (**B**), epicardial adipose tissue (EAT) volume index (**C**), and the combination of LVEF and LGE detection plus EAT volume index (**D**). Low EAT volume <2.2 mL*m^2/Kg, high EAT volume≥2.2 mL *m^2/Kg.*

5.8. Discussion

The main findings of this study are that in patients with known or suspected CAD undergoing CMR:

1) EAT can be automatically and accurately quantified using a new DL algorithm on standard short-axis cine CMR images with a performance comparable to human expert assessment.

2) EAT volume index is a strong and independent predictor of MACE with an incremental prognostic role on top of standard clinical and CMR parameters such as LVEF and LGE.

As anticipated EAT covers 80% of the heart surface and is more represented in the atrioventricular and interventricular grooves and around the epicardial coronary arteries [46]. Differently from the adipose tissues of other organs of the organism, EAT has specific anatomical and functional characteristics, it consists of adipocytes with brown or beige features and it is an active endocrine organ.[47]

A growing body of evidence suggests that EAT may contribute to developing obstructive CAD[48] and even acute coronary syndromes.[49] As a result of adversely remodeled and dysfunctional EAT, proinflammatory cytokines are released. It is well established that inflammation is strongly associated with all phases of CAD, from early atherogenesis to atherosclerotic plaque progression and, ultimately plaque rupture. [13,32]

CMR is considered the most effective non-invasive methods for measuring EAT and to distinguish it from paracardial adipose deposit.[50] In contrast to echocardiography,

CMR allows a 3D analysis of the EAT volume; moreover, differently from CCT, it does not require ionizing radiation.[40]

Yet, the use of CMR for EAT quantification appears to be limited and several authors have focused their efforts in quantifying EAT with non-contrast CCT.[30] Nelson described an accurate and reproducible CMR technique capable of measuring EAT.[9] The method, validated ex vivo in an ovine model, consists in tracing adipose tissue on consecutive SSFP cine end diastolic short-axis images, beginning with the most basal slice at the level of the mitral valve and moving apically to the most inferior margin of adipose tissue. The volume is then derived using a modified Simpson's rule.[9] Applying this method, CMR derived EAT has been investigated in small cohorts as an adverse cardiovascular imaging marker.

In a study on 64 heart failure patients with LVEF >40% undergoing routine CMR, patients with heart failure had more EAT compared to controls, despite similar body mass index. Moreover, EAT volume was associated with the presence of atrial fibrillation (AF), type 2 diabetes mellitus and with biomarkers related to myocardial injury.[28,51] Wang et al. studied 110 patients undergoing first-time AF ablation, demonstrating that EAT is associated with the presence of AF, the severity of AF, left atrial volumes, and poorer outcomes after AF ablation.[23] EAT volume has been also correlated with larger infarct size, microvascular obstruction, and greater ST-deviation.[52]

The time required for manual quantification of EAT is a limiting factor to the use of CMR for this purpose and, in contrast to CCT[53], there is little data on the use of artificial intelligence for quantifying EAT in CMR and on its potential prognostic role.

Ding et al. developed an algorithm for automated pericardial fat quantification based on water/fat-resolved whole-heart coronary magnetic resonance angiography.[54] In his study, however, only ten patients were analyzed. An expert reader segmented the images of just four patients, and the algorithm was applied to the remaining six subjects.[54]

Recently, a DL algorithm has been proposed for a fully automated quantification of the pericardial adipose tissue surrounding a standard CMR four-chamber.[55] The algorithm has subsequently been then applied to 42598 studies in the U.K. biobank[56] and has revealed an association between the pericardial adipose tissue measured with CMR and adverse cardiovascular structure (greater wall thickness, higher left ventricle mass, more concentric patterns of left ventricle remodeling), poorer left ventricle and left atrium function and lower arterial compliance.[56] Moreover, larger pericardial adipose tissue was associated with cardiometabolic diseases and blood biomarkers suggestive of poorer glycemic control, abnormal serum lipids, and proinflammatory markers.[56]

It should be noted that the pericardial fat measured in this latter study encompassed paracardial (adipose tissue situated between the visceral and parietal layers of the pericardium), epicardial, and pericardial fat (adipose tissue located externally to the parietal pericardium), whereas previous literature has identified EAT as the compartment more associated with cardiovascular risk and morbidity.[56] Furthermore, the pericardial adipose tissue was measured based on the area of fat rather than providing volumetric measurements. Finally, the study was conducted in the healthy population of the U.K. biobank, and no information about myocardial tissue characterization with CMR is provided.[56]

5.9. Strengths and clinical implications

Our study presents important elements of novelty in comparison to previous papers.

To begin with, it is the first study to demonstrate that the EAT volume can be accurately segmented and measured with fully automated DL algorithms on CMR cine SSFP images without additional time required for scanning or analysis.

Secondly, we have shown that CMR-derived EAT volume index has an additional predictive role for MACE over and above standard clinical and imaging parameters in a large population of patients with known or suspected CAD. In particular, we tested the additional role of EAT measurements in comparison with other common outcomes predictors including CMR tissue characterization with LGE technique. Surprisingly, we found an additional predictive role of EAT volume index even above LGE which is recognized as the strongest predictor of adverse cardiovascular events in both non-ischemic and ischemic cardiomyopathy.[57]

The results of our study may have important clinical implications. Indeed, by incorporating this DL algorithm into CMR imaging, EAT could be accurately and fully automatedly quantified by providing a robust method to assess patient's risk. There are virtually no limitations to the application of this algorithm to CMR studies. EAT is measured using short-axis cine SSFP stacks, which are routinely acquired in any CMR study for calculating biventricular dimension and function without the need for contrast agents. Furthermore, unlike manual quantification of EAT, which is time-consuming, the proposed algorithm allows epicardial fat to be quantified within a few seconds.

5.10. Limitations

Our study presents some limitations. Firstly, it is a single-center study with potential referral bias. In particular, we retrospectively enrolled patients with clinically indicated CMR with potential inclusion bias. In spite of this, our results are representative since we included a large number of patients and followed them for an extended period.

Secondly, the clinical utility of CMR derived from EAT will need to be demonstrated in other independent cohorts before it can be applied to clinical practice.

Thirdly, we did not use mapping sequences to characterize the myocardium. however, we tested the predictive role of EAT against LGE sequences which represent a known strong predictor of MACE. Eventually, CMR is, on average, less accessible compared to CCT scan and requires longer scan times.

In addition, there are specific CMR contraindications, such as patients with non-compatible devices or with claustrophobia, that do not limit the performance of CCT. Yet, the main advantage of CMR over CCT is that it does not use ionizing radiation.

5.11. Conclusion

EAT volume index measured with a DL algorithm in standard cine CMR images represents a robust independent predictor of MACE in patients with known or

suspected CAD. EAT volume index owns an additional prognostic role on top of standard clinical and imaging parameters.

Keywords

Epicardial adipose tissue; epicardial fat; coronary artery disease; deep learning; cardiac segmentation; cardiac magnetic resonance; outcome.

Abbreviations

ACE: angiotensin-converting enzyme; **AT1**: angiotensin II receptor 1; **BSA**: body surface area; **CABG**: coronary artery bypass graft; **CI**: confidence interval; **ESV**: end systolic volume; **LV**: left ventricle; **MACE**: major adverse cardiovascular events (myocardial infarction or cardiac death); **RV**: right ventricle; **SV**: stroke volume.

REFERENCES

1. Guglielmo M, Lin A, Dey D, et al. Epicardial fat and coronary artery disease: Role of cardiac imaging. *Atherosclerosis*. 2021;321:30-38. doi:10.1016/j.atherosclerosis.2021.02.008

2. Talman AH, Psaltis PJ, Cameron JD, Meredith IT, Seneviratne SK, Wong DTL. Epicardial adipose tissue: far more than a fat depot. *Cardiovasc Diagn Ther*. 2014;4(6).

3. Lin A, Dey D, Wong DTL, Nerlekar N. Perivascular Adipose Tissue and Coronary Atherosclerosis: from Biology to Imaging Phenotyping. *Curr Atheroscler Rep*. 2019;21(12):47. doi:10.1007/s11883-019-0817-3

4. Bos D, Shahzad R, Van Walsum T, et al. Epicardial fat volume is related to atherosclerotic calcification in multiple vessel beds. *Eur Heart J – Cardiovasc Imaging*. 2015;16(11):1264-1269. doi:10.1093/ehjci/jev086

5. Goeller M, Achenbach S, Cadet S, et al. Pericoronary Adipose Tissue Computed Tomography Attenuation and High-Risk Plaque Characteristics in Acute Coronary Syndrome Compared With Stable Coronary Artery Disease. *JAMA Cardiol*. 2018;3(9):858. doi:10.1001/jamacardio.2018.1997

6. Tamarappoo B, Dey D, Shmilovich H, et al. Increased Pericardial Fat Volume Measured From Noncontrast CT Predicts Myocardial Ischemia by SPECT. *JACC Cardiovasc Imaging*. 2010;3(11):1104-1112. doi:10.1016/j.jcmg.2010.07.014

7. Monti CB, Codari M, De Cecco CN, Secchi F, Sardanelli F, Stillman AE. Novel imaging biomarkers: epicardial adipose tissue evaluation. *Br J Radiol*. 2020;93(1113):20190770. doi:10.1259/bjr.20190770

8. Maragna R, Giacari CM, Guglielmo M, et al. Artificial Intelligence Based Multimodality Imaging: A New Frontier in Coronary Artery Disease Management. *Front Cardiovasc Med*. 2021;8:736223. doi:10.3389/fcvm.2021.736223

9. Nelson AJ, Worthley MI, Psaltis PJ, et al. Validation of cardiovascular magnetic resonance assessment of pericardial adipose tissue volume. *J Cardiovasc Magn Reson*. 2009;11(1):15. doi:10.1186/1532-429X-11-15

10. Marchington JM, Pond CM. SITE-SPECIFIC PROPERTIES OF PERICARDIAL AND EPICARDIAL ADIPOSE TISSUE: THE EFFECTS OF INSULIN AND HIGH-FAT FEEDING ON LIPOGENESIS AND THE INCORPORATION OF FATTY ACIDS IN VITRO.

11. Iacobellis G. Local and systemic effects of the multifaceted epicardial adipose tissue depot. *Nat Rev Endocrinol*. 2015;11(6):363-371. doi:10.1038/nrendo.2015.58

12. Mazurek T, Zhang L, Zalewski A, et al. Human Epicardial Adipose Tissue Is a Source of Inflammatory Mediators. *Circulation*. 2003;108(20):2460-2466. doi:10.1161/01.CIR.0000099542.57313.C5

13. Hirata Y, Tabata M, Kurobe H, et al. Coronary Atherosclerosis Is Associated With Macrophage Polarization in Epicardial Adipose Tissue. *J Am Coll Cardiol*. 2011;58(3):248-255. doi:10.1016/j.jacc.2011.01.048

14. Iacobellis G. Epicardial adipose tissue in contemporary cardiology. *Nat Rev Cardiol*. 2022;19(9):593-606. doi:10.1038/s41569-022-00679-9

15. Magnani JW, Rienstra M, Lin H, et al. Atrial Fibrillation: Current Knowledge and Future Directions in Epidemiology and Genomics. *Circulation*. 2011;124(18):1982-1993. doi:10.1161/CIRCULATIONAHA.111.039677

16. Yamaguchi Y, Cavallero S, Patterson M, et al. Adipogenesis and epicardial adipose tissue: A novel fate of the epicardium induced by mesenchymal transformation and PPARγ activation. *Proc Natl Acad Sci*. 2015;112(7):2070-2075. doi:10.1073/pnas.1417232112

17. Gaborit B, Venteclef N, Ancel P, et al. Human epicardial adipose tissue has a specific transcriptomic signature depending on its anatomical peri-atrial, peri-ventricular, or peri-coronary location. *Cardiovasc Res*. 2015;108(1):62-73. doi:10.1093/cvr/cvv208

18. Goldberger JJ, Arora R, Green D, et al. Evaluating the Atrial Myopathy Underlying Atrial Fibrillation: Identifying the Arrhythmogenic and Thrombogenic

Substrate. *Circulation*. 2015;132(4):278-291. doi:10.1161/CIRCULATIONAHA.115.016795

19. Munger TM, Dong YX, Masaki M, et al. Electrophysiological and Hemodynamic Characteristics Associated With Obesity in Patients With Atrial Fibrillation. *J Am Coll Cardiol*. 2012;60(9):851-860. doi:10.1016/j.jacc.2012.03.042

20. Nalliah CJ, Bell JR, Raaijmakers AJA, et al. Epicardial Adipose Tissue Accumulation Confers Atrial Conduction Abnormality. *J Am Coll Cardiol*. 2020;76(10):1197-1211. doi:10.1016/j.jacc.2020.07.017

21. Nagashima K, Okumura Y, Watanabe I, et al. Association Between Epicardial Adipose Tissue Volumes on 3-Dimensional Reconstructed CT Images and Recurrence of Atrial Fibrillation After Catheter Ablation. *Circ J*. 2011;75(11):2559-2565. doi:10.1253/circj.CJ-11-0554

22. Pathak RK, Middeldorp ME, Lau DH, et al. Aggressive Risk Factor Reduction Study for Atrial Fibrillation and Implications for the Outcome of Ablation. *J Am Coll Cardiol*. 2014;64(21):2222-2231. doi:10.1016/j.jacc.2014.09.028

23. Wong CX, Abed HS, Molaee P, et al. Pericardial Fat Is Associated With Atrial Fibrillation Severity and Ablation Outcome. *J Am Coll Cardiol*. 2011;57(17):1745-1751. doi:10.1016/j.jacc.2010.11.045

24. Masuda M, Mizuno H, Enchi Y, et al. Abundant epicardial adipose tissue surrounding the left atrium predicts early rather than late recurrence of atrial fibrillation after catheter ablation. *J Interv Card Electrophysiol*. 2015;44(1):31-37. doi:10.1007/s10840-015-0031-3

25. Kocyigit D, Gurses KM, Yalcin MU, et al. Periatrial epicardial adipose tissue thickness is an independent predictor of atrial fibrillation recurrence after cryoballoon-based pulmonary vein isolation. *J Cardiovasc Comput Tomogr*. 2015;9(4):295-302. doi:10.1016/j.jcct.2015.03.011

26. Wong CX, Ganesan AN, Selvanayagam JB. Epicardial fat and atrial fibrillation: current evidence, potential mechanisms, clinical implications, and future directions. *Eur Heart J*. Published online March 1, 2016:ehw045. doi:10.1093/eurheartj/ehw045

27. Yancy CW, Jessup M, Bozkurt B, et al. 2017 ACC/AHA/HFSA Focused Update of the 2013 ACCF/AHA Guideline for the Management of Heart Failure: A Report of the American College of Cardiology/American Heart Association Task Force on Clinical Practice Guidelines and the Heart Failure Society of America. *Circulation*. 2017;136(6). doi:10.1161/CIR.0000000000000509

28. Van Woerden G, Gorter TM, Westenbrink BD, Willems TP, Van Veldhuisen DJ, Rienstra M. Epicardial fat in heart failure patients with mid-range and preserved ejection fraction. *Eur J Heart Fail*. 2018;20(11):1559-1566. doi:10.1002/ejhf.1283

29. Fontes-Carvalho R, Fontes-Oliveira M, Sampaio F, et al. Influence of Epicardial and Visceral Fat on Left Ventricular Diastolic and Systolic Functions in Patients After Myocardial Infarction. *Am J Cardiol*. 2014;114(11):1663-1669. doi:10.1016/j.amjcard.2014.08.037

30. Spearman JV, Renker M, Schoepf UJ, et al. Prognostic value of epicardial fat volume measurements by computed tomography: a systematic review of the literature. *Eur Radiol*. 2015;25(11):3372-3381. doi:10.1007/s00330-015-3765-5

31. De Vos AM, Prokop M, Roos CJ, et al. Peri-coronary epicardial adipose tissue is related to cardiovascular risk factors and coronary artery calcification in post-menopausal women. *Eur Heart J*. 2008;29(6):777-783. doi:10.1093/eurheartj/ehm564

32. Liu Z, Wang S, Wang Y, et al. Association of epicardial adipose tissue attenuation with coronary atherosclerosis in patients with a high risk of coronary artery disease. *Atherosclerosis*. 2019;284:230-236. doi:10.1016/j.atherosclerosis.2019.01.033

33. Iacobellis G, Mahabadi AA. Is epicardial fat attenuation a novel marker of coronary inflammation? *Atherosclerosis*. 2019;284:212-213. doi:10.1016/j.atherosclerosis.2019.02.023

34. Franssens BT, Nathoe HM, Leiner T, Van Der Graaf Y, Visseren FL. Relation between cardiovascular disease risk factors and epicardial adipose tissue density on cardiac computed tomography in patients at high risk of cardiovascular events. *Eur J Prev Cardiol*. 2017;24(6):660-670. doi:10.1177/2047487316679524

35. Attanasio S, Forte SM, Restante G, Gabelloni M, Guglielmi G, Neri E. Artificial intelligence, radiomics and other horizons in body composition assessment. *Quant Imaging Med Surg*. 2020;10(8):1650-1660. doi:10.21037/qims.2020.03.10

36. Moccia S, Banali R, Martini C, et al. Development and testing of a deep learning-based strategy for scar segmentation on CMR-LGE images. *Magn Reson Mater Phys Biol Med*. 2019;32(2):187-195. doi:10.1007/s10334-018-0718-4

37. Shelhamer E, Long J, Darrell T. Fully Convolutional Networks for Semantic Segmentation. *IEEE Trans Pattern Anal Mach Intell*. 2017;39(4):640-651. doi:10.1109/TPAMI.2016.2572683

38. Alshazly H, Linse C, Barth E, Martinetz T. Handcrafted versus CNN Features for Ear Recognition. *Symmetry*. 2019;11(12):1493. doi:10.3390/sym11121493

39. Paszke A, Chaurasia A, Kim S, Culurciello E. ENet: A Deep Neural Network Architecture for Real-Time Semantic Segmentation. Published online June 7, 2016. Accessed October 14, 2023. http://arxiv.org/abs/1606.02147

40. Pohost GM, Kim RJ, Kramer CM, Manning WJ. Task Force 12: Training in Advanced Cardiovascular Imaging (Cardiovascular Magnetic Resonance [CMR]). *J Am Coll Cardiol*. 2008;51(3):404-408. doi:10.1016/j.jacc.2007.11.020

41. Brendel JM, Holtackers RJ, Geisel JN, et al. Dark-Blood Late Gadolinium Enhancement MRI Is Noninferior to Bright-Blood LGE in Non-Ischemic Cardiomyopathies. *Diagnostics*. 2023;13(9):1634. doi:10.3390/diagnostics13091634

42. Karim R, Bhagirath P, Claus P, et al. Evaluation of state-of-the-art segmentation algorithms for left ventricle infarct from late Gadolinium enhancement MR images. *Med Image Anal*. 2016;30:95-107. doi:10.1016/j.media.2016.01.004

43. Ronneberger O, Fischer P, Brox T. U-Net: Convolutional Networks for Biomedical Image Segmentation. Published online May 18, 2015. Accessed October 14, 2023. http://arxiv.org/abs/1505.04597

44. Shelhamer E, Long J, Darrell T. Fully Convolutional Networks for Semantic Segmentation. *IEEE Trans Pattern Anal Mach Intell*. 2017;39(4):640-651. doi:10.1109/TPAMI.2016.2572683

45. Penso M, Moccia S, Scafuri S, et al. Automated left and right ventricular chamber segmentation in cardiac magnetic resonance images using dense fully convolutional neural network. *Comput Methods Programs Biomed*. 2021;204:106059. doi:10.1016/j.cmpb.2021.106059

46. Rabkin SW. Epicardial fat: properties, function and relationship to obesity. *Obes Rev*. 2007;8(3):253-261. doi:10.1111/j.1467-789X.2006.00293.x

47. Iacobellis G, Bianco AC. Epicardial adipose tissue: emerging physiological, pathophysiological and clinical features. *Trends Endocrinol Metab*. 2011;22(11):450-457. doi:10.1016/j.tem.2011.07.003

48. Zhou J, Chen Y, Zhang Y, et al. Epicardial Fat Volume Improves the Prediction of Obstructive Coronary Artery Disease Above Traditional Risk Factors and Coronary Calcium Score: Development and Validation of New Pretest Probability Models in Chinese Populations. *Circ Cardiovasc Imaging*. 2019;12(1):e008002. doi:10.1161/CIRCIMAGING.118.008002

49. Tscharre M, Hauser C, Rohla M, et al. Epicardial adipose tissue and cardiovascular outcome in patients with acute coronary syndrome undergoing percutaneous

coronary intervention. *Eur Heart J Acute Cardiovasc Care*. 2017;6(8):750-752. doi:10.1177/2048872616680609

50. Flüchter S, Haghi D, Dinter D, et al. Volumetric Assessment of Epicardial Adipose Tissue With Cardiovascular Magnetic Resonance Imaging*. *Obesity*. 2007;15(4):870-878. doi:10.1038/oby.2007.591

51. Conte M, Petraglia L, Cabaro S, et al. Epicardial Adipose Tissue and Cardiac Arrhythmias: Focus on Atrial Fibrillation. *Front Cardiovasc Med*. 2022;9:932262. doi:10.3389/fcvm.2022.932262

52. Fisser C, Colling S, Debl K, et al. The impact of epicardial adipose tissue in patients with acute myocardial infarction. *Clin Res Cardiol*. 2021;110(10):1637-1646. doi:10.1007/s00392-021-01865-4

53. Greco F, Salgado R, Van Hecke W, Del Buono R, Parizel PM, Mallio CA. Epicardial and pericardial fat analysis on CT images and artificial intelligence: a literature review. *Quant Imaging Med Surg*. 2022;12(3):2075-2089. doi:10.21037/qims-21-945

54. Ding X, Pang J, Ren Z, et al. Automated pericardial fat quantification from coronary magnetic resonance angiography: feasibility study. *J Med Imaging*. 2016;3(1):014002. doi:10.1117/1.JMI.3.1.014002

55. Bard A, Raisi-Estabragh Z, Ardissino M, et al. Automated Quality-Controlled Cardiovascular Magnetic Resonance Pericardial Fat Quantification Using a Convolutional Neural Network in the UK Biobank. *Front Cardiovasc Med*. 2021;8:677574. doi:10.3389/fcvm.2021.677574

56. Ardissino M, McCracken C, Bard A, et al. Pericardial adiposity is independently linked to adverse cardiovascular phenotypes: a CMR study of 42 598 UK Biobank participants. *Eur Heart J - Cardiovasc Imaging*. 2022;23(11):1471-1481. doi:10.1093/ehjci/jeac101

57. Ganesan AN, Gunton J, Nucifora G, McGavigan AD, Selvanayagam JB. Impact of Late Gadolinium Enhancement on mortality, sudden death and major adverse cardiovascular events in ischemic and nonischemic cardiomyopathy: A systematic review and meta-analysis. *Int J Cardiol*. 2018;254:230-237. doi:10.1016/j.ijcard.2017.10.094